Journal of Catalysis **208,** 211–223 (2002)
doi:10.1006/jcat.2002.3559, available online at http://www.idealibrary.com on IDEAL®

NO-Assisted N_2O Decomposition over Fe-Based Catalysts: Effects of Gas-Phase Composition and Catalyst Constitution

Javier Pérez-Ramírez,[1] Freek Kapteijn, Guido Mul, and Jacob A. Moulijn

Industrial Catalysis, DelftChemTech, Delft University of Technology, Julianalaan 136, 2628 BL, Delft, The Netherlands

Received November 21, 2001; revised February 7, 2002; accepted February 7, 2002

The decomposition of N_2O is strongly promoted by NO over Fe catalysts supported on zeolites (*ex*-framework FeMFI catalysts, sublimed Fe/ZSM-5, ion-exchanged Fe–ZSM-5, Fe-beta, and Fe–USY) and conventional supports (Fe/Al_2O_3 and Fe/SiO_2) in a wide temperature range (550–900 K). Mixtures of NO and O_2 in the N_2O-containing feed lead to the same promoting effect as NO only. The promoting effect of NO is catalytic, and in addition to NO_2, O_2 is formed much more extensively at lower temperatures than in the absence of NO. The promotion effect only requires low NO concentrations in the feed, with no significant improvements at molar NO/N_2O feed ratios higher than 0.25. No inhibition by NO was identified even at a molar NO/N_2O feed ratio of 10, suggesting different sites for NO adsorption and oxygen deposition by N_2O. The latter sites seem to be remote from each other. Multitrack experiments on *ex*-framework FeZSM-5 show that release of oxygen from the catalyst surface during direct N_2O decomposition is a rate-determining step, due to the slow oxygen recombination, which is favored by high reaction temperatures. NO addition promotes this oxygen desorption. Adsorbed NO accommodates oxygen from N_2O and the formed adsorbed NO_2 can react with a second oxygen from the neighboring site, thus accelerating the recombination of oxygen from N_2O. Less than 0.9% of the Fe seems to participate in this promotion. Adsorbed NO may even facilitate the migration of atomic oxygen to enhance their recombination. A model is proposed to explain the phenomena observed in the NO-assisted N_2O decomposition, including NO_2 decomposition.

Key Words: **N_2O decomposition; NO; Fe catalysts; FeZSM-5; *ex*-framework; Fe-beta; Fe–USY; Fe/Al_2O_3; promotion; O_2 desorption; mechanism; TAP reactor; transient kinetics.**

INTRODUCTION

Fe-based zeolite catalysts are currently extensively studied, because of high activity in (i) selective catalytic reduction of NO and N_2O with hydrocarbons or ammonia (1–8), (ii) N_2O-mediated selective oxidation of benzene to phenol (9–11), and (iii) direct catalytic N_2O decomposition (12–14), and selective oxidation of NH_3 to N_2 (15). We recently reported the extraordinary performance of a specific FeZSM-5 catalyst prepared via an *ex*-framework method in the N_2O decomposition reaction (16). The *ex*-framework catalyst (on a per Fe basis) shows a significantly higher activity than catalysts prepared via other procedures, such as liquid (aqueous)- or solid-ion exchange, or sublimation. Also the stability of this particular catalyst in simulated tail-gas mixtures from nitric acid plants and fluidized-bed combustors is excellent (16, 17).

An intriguing general feature of FeZSM-5 catalysts in N_2O decomposition is that NO significantly enhances the activity, while the opposite effect is usually observed for other catalytic systems, e.g., those based on noble metals (Ru or Rh) (18, 19). This peculiar behavior of FeZSM-5 makes it very attractive to use in applications where both N_2O and NO are present, such as in tail gas of nitric acid plants. The positive effect of NO and also of SO_2 on the N_2O conversion was first reported by some of us in 1996, using a FeZSM-5 prepared by liquid (aqueous)-ion exchange with Fe(II) sulfate (20). At that time it was proposed that NO in the gas phase scavenged adsorbed oxygen (deposited by N_2O during the oxidation of active sites, Eq. [1]), leading to the formation of NO_2 and regeneration of the active site (Eq. [2]).

$$N_2O + * \rightarrow N_2 + O^* \quad [1]$$

$$NO + O^* \rightarrow NO_2 + * \quad [2]$$

Reduction of an oxidized site by NO as represented in Eq. [2] should lead to a stoichiometric process in which NO and N_2O react to form N_2 and NO_2:

$$N_2O + NO \rightarrow N_2 + NO_2. \quad [3]$$

Recently we reported transient experiments using FT-IR/MS (Fourier transform infrared coupled to mass spectrometry) and Multitrack (multiple time resolved analysis of catalytic kinetics), an advanced TAP-reactor, to further analyze the NO-assisted N_2O decomposition over *ex*-framework FeZSM-5 (21). It was shown that besides NO_2 formation, enhanced O_2 formation is involved. It was proposed that the latter is either an indirect effect (electronic or steric) of NO adsorbed on sites neighboring the N_2O

[1] To whom correspondence should be addressed. Current address: Norsk Hydro, Research Centre, P.O. Box 2560, N-3907, Porsgrunn, Norway. Fax: 47 35 923043. E-mail: javier.perez.ramirez@hydro.com.

0021-9517/02 $35.00

decomposition sites, or a direct effect involving reaction of adsorbed NO_2 groups with neighboring oxidized sites yielding O_2.

In this paper it is shown that NO-assisted N_2O decomposition is not a special feature of FeZSM-5 catalysts, but a general phenomenon occurring over many Fe-containing zeolitic and nonzeolitic catalysts. Furthermore, additional activity data on the effect of the molar NO/N_2O ratio and reaction temperature on the performance of these catalysts is presented. Based on flow and pulse experiments, steady-state and transient phenomena regarding the chemistry of N_2O, NO, and NO_2 over Fe catalysts are investigated, and possible catalytic cycles in NO-assisted N_2O decomposition are proposed.

EXPERIMENTAL

Catalysts

The chemical compositions of the different catalysts used in this study are summarized in Table 1.

Ex-framework Fe catalysts. Isomorphously substituted FeMFI was synthesized hydrothermally using tetrapropylammonium hydroxide as the template (11). The molar ratios between the components was $H_2O/Si = 45$, TPAOH/$Si = 0.3$, $Si/Al = 36$, and $Si/Fe = 152$. The as-synthesized sample, in which Fe(III) is isomorphously substituted in the zeolite framework, was calcined in air at 823 K for 10 h and was then converted into the H form by three consecutive exchanges with an ammonium nitrate solution (0.1 M) overnight and subsequent calcination at 823 K for 5 h. Finally, the catalyst was treated in flowing steam at ambient pressure (water partial pressure of 300 mbar and 30 $ml \cdot min^{-1}$ of N_2 flow) at 873 K over the course of 5 h, yielding a sample denoted *ex*-[Fe,Al]MFI(a).

In a modified synthesis route, *ex*-[Fe,Al]MFI was prepared using the same molar metal ratios but a lower molar TPAOH/Si ratio (0.1 instead of 0.3). This was done by adding NaOH to the synthesis gel in a molar NaOH/Si ratio of 0.2 (denoted *ex*-[Fe,Al]MFI(b)). Following this route, ferrigallosilicate (denoted *ex*-[Fe,Ga]MFI) and ferrisilicate (denoted *ex*-[Fe]MFI) were also prepared. Addition of NaOH to the synthesis gel induces a lower template concentration and thus a larger crystal size for the final catalysts (0.4 μm in *ex*-[Fe,Al]MFI(a) vs 2.0–2.5 μm in *ex*-[Fe,Al]MFI(b), *ex*-[Fe,Ga]MFI, and *ex*-[Fe]MFI catalysts). More details on the preparation methods and characterization of these materials can be found elsewhere (11).

TABLE 1

Chemical Composition of the Catalysts Used in this Study

Catalyst	Method	Si/Al or Si/Ga[a]	Fe[a] (wt%)
ex-[Fe,Al]MFI(a)	*Ex*-framework	32.6	0.66
ex-[Fe,Al]MFI(b)	*Ex*-framework	32.6	0.64
ex-[Fe,Ga]MFI	*Ex*-framework	32.6	0.58
ex-[Fe]MFI	*Ex*-framework	—	0.68
Fe/ZSM-5	Sublimation	14.0	5.0
Fe–ZSM-5	Ion exchange	37.5	1.44
Fe-beta	Ion exchange	11.0	1.50
Fe–USY	Ion exchange	15.5	1.28
Fe/Al_2O_3	Incipient wetness	—	2.0
Fe/SiO_2	Incipient wetness	—	2.0

[a] Determined by ICP–OES.

Other Fe catalysts. Fe/ZSM-5 was prepared by sublimation of $FeCl_3$ on HZSM-5 (Degussa, $Si/Al = 14.0$), according to the method described by Chen and Sachtler (2). Fe–ZSM-5, Fe-beta, and Fe–USY were prepared by liquid (aqueous)-ion exchanged with diluted solutions (0.30 mM) of $Fe(NO_3)_3 \cdot 9H_2O$ (Fe–ZSM-5 and Fe–USY) and $FeSO_4 \cdot 7H_2O$ (Fe-beta). The parent zeolites were provided by Zeolyst (NH_4–ZSM-5, CBV8020, $Si/Al = 37.5$; beta, CP814E, $Si/Al = 11$; H–USY, CBV720, $Si/Al = 15.5$). The exchange was carried out under vigorous stirring over the course of 15 h. The zeolites were then filtered, washed thoroughly, dried, and finally calcined in static air at 825 K for 5 h. Fe/Al_2O_3 and Fe/SiO_2 were prepared by incipient wetness impregnation, with appropriate aqueous solutions of iron(II) gluconate, $Fe[OHCH_2(CHOH)_4CO_2]_2 \cdot 2H_2O$. Al_2O_3 (CK300) and SiO_2 were purchased from Ketjen and Grace, respectively. After the impregnation the samples were dried at 363 K, followed by calcination at 493 K for 1 h and at 773 K for 5 h.

Activity Tests

Activity measurements were carried out in a six-flow reactor system (22), using 50 mg of catalyst (125–200 μm) and a space velocity (GHSV) of 60,000 h^{-1} at atmospheric pressure. The feed conditions used were 1.5 mbar of N_2O, 0–15 mbar of NO, 0–0.2 mbar of NO_2, and 0–20 mbar of O_2, with He as balance gas. Before reaction, the catalysts were pretreated in N_2O (1.5 mbar of N_2O in He) at 723 K for 1 h and cooled in that gas flow to the initial reaction temperature. In the temperature range of 550–925 K, deactivation of the catalysts was absent. N_2O, N_2, and O_2 were analyzed with a GC (Chrompack CP 9001) equipped with a thermal conductivity detector, using a Poraplot Q column (for N_2O separation) and a Molsieve 5A column (for N_2 and O_2 separation). NO, NO_2, and NO_x concentrations were determined with a chemiluminescence NO_x analyzer (Ecophysics CLD 700 EL).

Multitrack Experiments

Experimental setup. A detailed description of the Multitrack system, a TAP-reactor-like high-vacuum reactor system suited for pulse experiments, is presented elsewhere (23). Two different gases can be dosed to the reactor by means of high-speed pulse valves, yielding pulses of

10^{17} molecules within 100 μs. The reactor with the catalyst sample is located in a high-vacuum system, and during pulsing the peak pressure remains below 3 Pa. The catalyst bed (100 mg; pellet size, 125–200 μm) is packed between two layers of inert SiC particles (particle size, 230 μm), consisting of 200 and 125 mg before and after the bed, respectively. In the reactor, the shape and composition of the gas pulse change due to processes such as diffusion, adsorption, and reaction. At the reactor exit the reaction products are analyzed by four quadrupole mass spectrometers positioned in line with the reactor axis. All mass spectrometers are able to analyze one of the components (m/e unit) in the exit gas stream with a maximum sample frequency of 1 MHz. In this study most analyses were carried out with the mass spectrometer located closest to the exit of the catalytic reactor. As the signal-to-noise ratio of this system is excellent, single pulses are sufficient to obtain good peak signals. This is an important aspect, as transient phenomena may remain unobserved when several pulse responses have to be averaged.

Procedure. Several types of Multitrack experiments were performed with *ex*-[Fe,Al]MFI(a). Before the measurements, the *ex*-[Fe,Al]MFI(a) catalyst was evacuated in the Multitrack reactor at 723 K for 3 h. The mechanistic studies of direct N_2O decomposition were carried out by continuously pulsing pure N_2O (~160 nmol) at intervals of 2 s ("cycle time") at different temperatures in the range of 623–973 K and recording the masses m/e 28 (N_2), m/e 32 (O_2), and m/e 44 (N_2O). Isothermal O_2 desorption was followed as a function of time after stopping N_2O pulsing (usually after ~100 pulses) in the temperature range of 673–798 K. The effect of NO on the N_2O decomposition was studied in dual-pulse experiments, in which pulses of N_2O (pure, ~160 nmol) and NO (15 vol% NO in Ar, ~24 nmol NO) are sequentially fed to the reactor with a time interval of 1 s between the pulses and a cycle time of 2 s. Isothermal transient desorption effects after stopping N_2O or NO pulsing were followed at different temperatures, ranging from 698 to 923 K. In these experiments, the masses m/e 30 (NO) and m/e 46 (NO_2) were additionally analyzed. The purity of the gases was >99.985%.

RESULTS

Activity Data

Ex-framework catalysts. The N_2O decomposition activity of *ex*-[Fe,Al]MFI(a) in different feed mixtures is presented in Fig. 1. In a N_2O/He feed, the catalyst shows a substantial N_2O conversion only above 700 K. Addition of NO (0.4 mbar; $NO/N_2O = 0.27$) enhances the reaction rate considerably. The N_2O conversion curve is shifted to temperatures about 100 K lower. The presence of oxygen (20 mbar of O_2) in the feed ($N_2O + NO + O_2$ in He) hardly affects the catalyst activity. The same promotion effect was obtained over the other *ex*-framework catalysts (Fig. 2). For these catalysts, the trend in activity in the N_2O–He feed (*ex*-[Fe,Al]MFI(b) + *ex*-[Fe,Ga]MFI > *ex*-[Fe]MFI) is maintained when NO is added to the feed mixture. For the different Fe–zeolites, the promotion effect by NO on the N_2O conversion also leads to a significant decrease in the apparent activation energy (Table 2), which has been estimated around the inflection of the activity vs temperature curves by assuming a plug-flow model and a first-order reaction in N_2O.

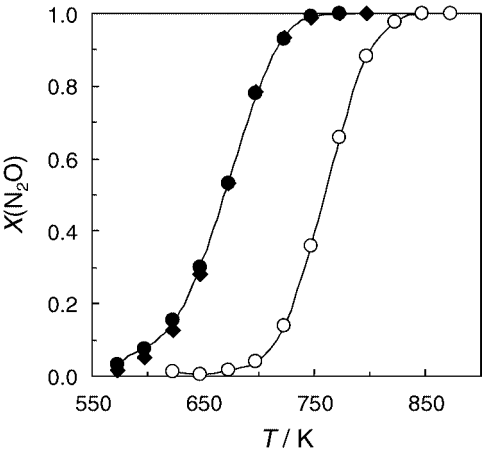

FIG. 1. N_2O conversion vs temperature over *ex*-[Fe,Al]MFI(a) in different feed compositions: (○) 1.5 mbar of N_2O in He, (●) 1.5 mbar of $N_2O + 0.4$ mbar NO in He, (◆) 1.5 mbar of $N_2O + 0.4$ mbar of $NO + 20$ mbar of O_2 in He; $P = 1$ bar; GHSV = 60,000 h^{-1}.

Figure 3 shows the influence of the molar NO/N_2O ratio in the feed on the N_2O conversion at reaction temperatures ranging from 623 to 723 K. N_2O conversion is dramatically improved at low NO partial pressures ($NO/N_2O < 0.25$).

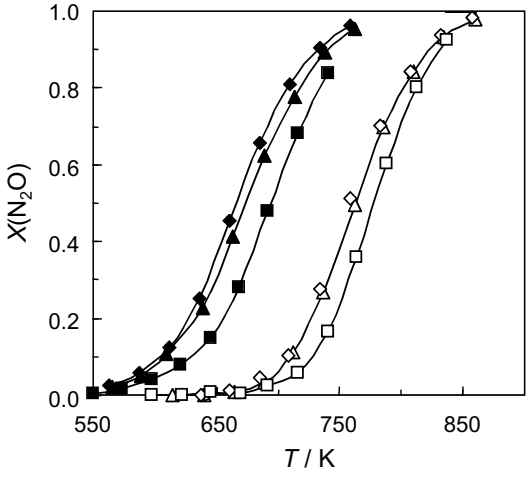

FIG. 2. N_2O conversion vs temperature over (◇, ◆) *ex*-[Fe,Al]MFI(b), (△, ▲) *ex*-[Fe,Ga]MFI, and (□, ■) *ex*-[Fe]MFI. Feed compositions: (◇, △, □) 1.5 mbar of N_2O in He and (◆, ▲, ■) 1.5 mbar of N_2O + 0.2 mbar of NO in He; $P = 1$ bar; GHSV = 60,000 h^{-1}.

TABLE 2

Apparent Activation Energy (E_a^{app}) of the *Ex*-Framework Catalysts for Direct N_2O Decomposition in the Absence or Presence of NO in the Feed Gas

Catalyst	E_a^{app}, N_2O[a] (kJ mol^{-1})	E_a^{app}, $N_2O + NO$[b] (kJ mol^{-1})
ex-[Fe,Al]MFI(a)	161	106
ex-[Fe,Al]MFI(b)	137	90
ex-[Fe,Ga]MFI	141	90
ex-[Fe]MFI	155	100

[a] Feed: 1.5 mbar N_2O in He; $P = 1$ bar; GHSV = 60,000 h^{-1}.
[b] Feed: 1.5 mbar N_2O + 0.2 mbar NO in He; $P = 1$ bar; GHSV = 60,000 h^{-1}.

From this value up to $NO/N_2O = 10$, little effect on N_2O conversion is noticed.

The NO, NO_2, and NO_x profiles provide further information on the effect of NO on the catalytic performance. In a N_2O + NO/He feed, the formation of NO_2 over *ex*-[Fe,Al]MFI(a) increases as a function of reaction temperature (Fig. 4), reaching a maximum at 650–675 K, i.e., around the inflection point of the N_2O decomposition activity curve (Fig. 1). Above this temperature, NO_2 formation decreases before completely disappearing at 775 K. The total NO_x level is constant in the temperature range investigated, indicating that NO_x is not converted to N_2 or N_2O. The amount of NO_2 formed is beyond the thermodynamic equilibrium of the NO and O_2 reaction (Eq. [4]), suggesting that the rate of the N_2O and NO reaction is higher than the decomposition rate of NO_2 over the catalyst. The equilibrium composition of NO_2 was calculated in two ways. If the oxygen present at a certain temperature (generated during N_2O decomposition) is used, the short dashed line in Fig. 4 is calculated. Equilibrium composition of NO and NO_2 was also determined assuming an O_2 availability corresponding to what the amount would be if N_2O conversion were 100% ($p(O_2) = 0.75$ mbar). These theoretical partial pressure profiles of NO and NO_2 are displayed in Fig. 4 by the long dashed lines. The occurrence of the N_2O and NO reaction should be attributed to the catalytic performance of *ex*-[Fe,Al]MFI(a), since no NO_2 formation was observed over an inert material (SiC) in the same feed composition (not shown).

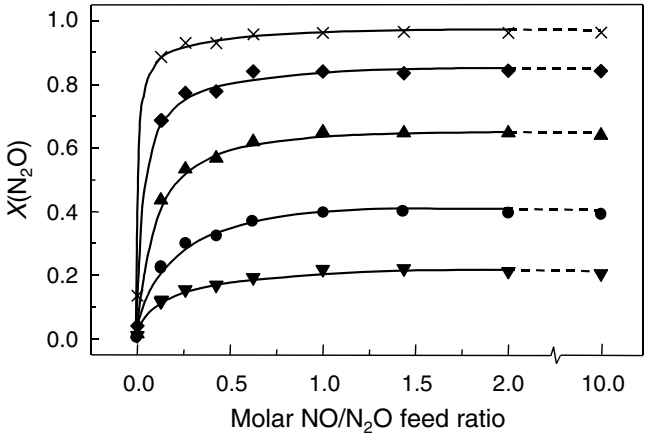

FIG. 3. N_2O conversion vs the molar NO/N_2O feed ratio over *ex*-[Fe,Al]MFI(a) at different temperatures: (▼) 623, (●) 648, (▲) 673, (◆) 698, and (×) 723 K. Partial N_2O pressure was fixed at 1.5 mbar and partial NO pressure varied from 0 to 15 mbar. $P = 1$ bar; GHSV = 60,000 h^{-1}.

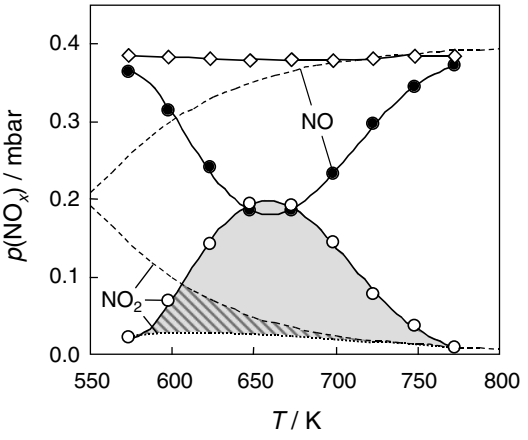

FIG. 4. Partial pressure of (●) NO, (○) NO_2, and (◇) NO_x vs temperature over *ex*-[Fe,Al]MFI(a). Feed composition: 1.5 mbar of N_2O + ~0.4 mbar of NO in He; $P = 1$ bar; GHSV = 60,000 h^{-1}. Equilibrium composition of NO and NO_2 (Eq. [4]) is represented by dashed lines (see text for details).

$$2NO + O_2 \rightleftharpoons 2NO_2 \qquad [4]$$

The profiles for *ex*-[Fe,Al]MFI(a) in a mixture of N_2O + NO + O_2/He are shown in Fig. 5a. The obtained NO/NO_2 ratio at low temperatures (~575 K) is lower than in the absence of O_2. In the presence of oxygen a larger fraction of NO in the feed mixture is oxidized to NO_2 (compare profiles in Figs. 4 and 5a). Again, the amount of NO_2 produced by the N_2O and NO reaction is beyond the thermodynamic equilibrium in Eq. [4] (taking 0.4 mbar of NO and 20 mbar of O_2 in He as input values in the calculation), while the presence of large amounts of oxygen shifts the theoretical equilibrium composition to higher NO_2 concentrations. However, comparing the profiles in Figs. 5a and 5b indicates that oxidation of NO to NO_2 occurs to a lesser extent in the absence of N_2O. In the NO oxidation with O_2 (Fig. 5b) the equilibrium composition of NO_2 was reached above 650 K and was not exceeded, which somehow indicates that the behavior observed in Figs. 4 and 5a is caused by a reaction between NO and N_2O.

In Fig. 6 the amount of NO_2 produced (solid diamonds) and O_2 produced (open circles) is plotted vs the amount of N_2O reacted to N_2 at 700 K for different inlet partial NO pressures. These results clearly show that the stoichiometric reaction of N_2O with NO to NO_2 and N_2 (Eq. [3]) cannot

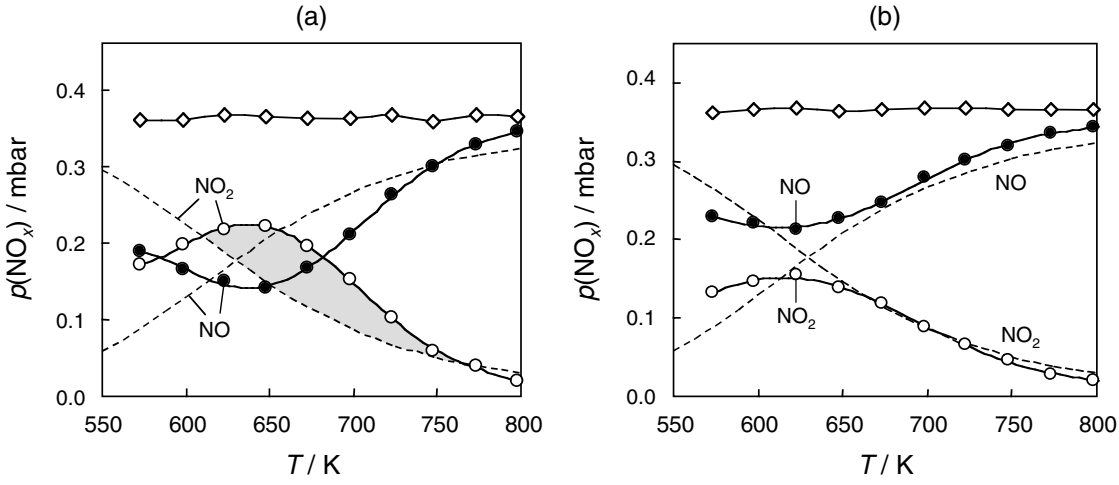

FIG. 5. Partial pressure of (●) NO, (○) NO_2, and (◇) NO_x vs temperature over *ex*-[Fe,Al]MFI(a). Feed composition: (a) 1.5 mbar of $N_2O + 0.4$ mbar of $NO + 20$ mbar of O_2 in He, and (b) 0.4 mbar of $NO + 20$ mbar of O_2 in He; $P = 1$ bar; GHSV = 60,000 h^{-1}. Equilibrium composition of NO and NO_2 (Eq. [4]) is represented by dashed lines.

solely explain the promotion effect observed in Figs. 1 and 2. Besides inducing the formation of NO_2, the presence of NO in the N_2O-containing feed also significantly enhances the production of O_2, closing the oxygen mass balance (long dashed line in Fig. 6).

Further information on the relatively low amount of NO_2 formed compared to the amount of N_2O decomposed can be related to the decomposition reaction of NO_2 to NO and O_2. By feeding a mixture of NO_2 in He over *ex*-[Fe,Al]MFI(a), the NO_2 decomposition rate was analyzed. The result for $p(NO_2)_o = 0.2$ mbar is shown in Fig. 7. NO_2 is converted into NO and O_2 over *ex*-[Fe,Al]MFI(a) in the temperature range where the promotion effect of NO occurs. Equilibrium is reached above 700 K, which indicates that NO_2 decomposition and NO oxidation by O_2 (Eq. [4]) occur fairly fast. This result suggests that NO_2 decomposition might contribute to the formation of O_2. Production of NO is hardly observed over inert material (SiC, not shown).

Other Fe catalysts. Figure 8 shows that the promotion effect of NO is not a unique feature of *ex*-framework Fe–zeolite catalysts. Sublimed Fe/ZSM-5, Fe–ZSM-5, Fe-beta, and Fe–USY catalysts prepared by liquid (aqueous)-ion exchange (Fig. 8a), as well as Fe supported on Al_2O_3 and SiO_2 (Fig. 8b) all show a significant enhancement of the N_2O conversion when NO is added to the feed. The observed beneficial effect of NO is larger for Fe–zeolites than for Fe/Al_2O_3 and Fe/SiO_2, manifested by a larger shift in operation

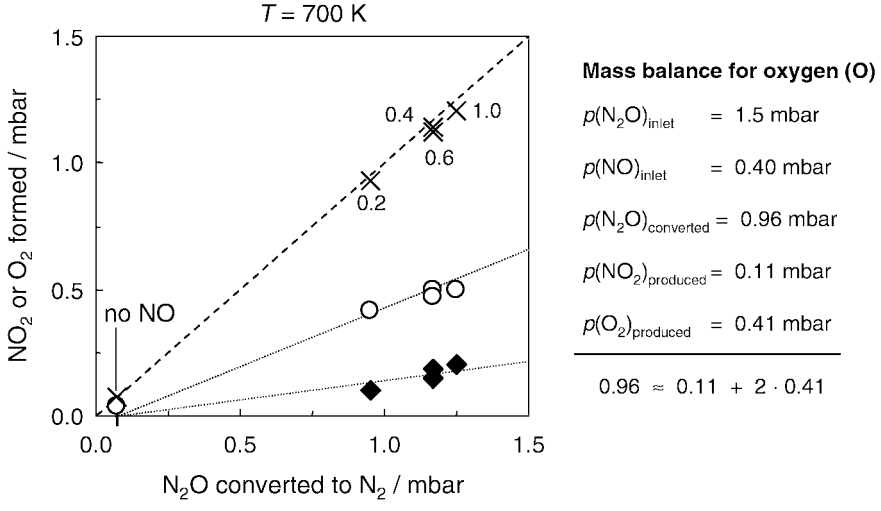

FIG. 6. NO_2 (◆) and O_2 (○) formed vs N_2O converted at 700 K over *ex*-[Fe,Al]MFI(a) at different partial NO pressures (mbar) in the feed. Crosses (×) represent the $NO_2 + O_2$ measured experimentally and the diagonal dashed line the mass balance for oxygen. The numbers refer to the NO/N_2O ratio in the feed. Feed composition: 1.5 mbar of N_2O + (0–1 mbar of NO) in He; $P = 1$ bar; GHSV = 60,000 h^{-1}.

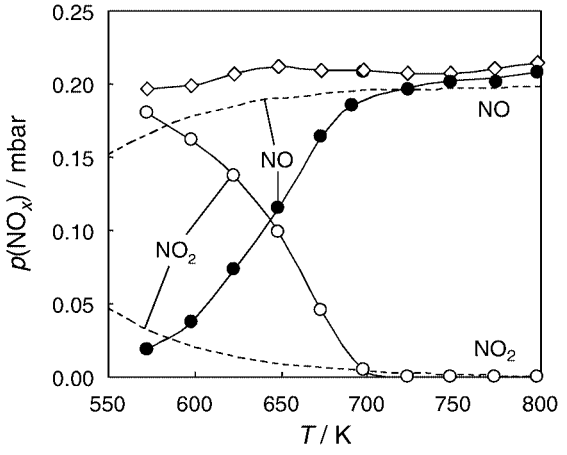

FIG. 7. Partial pressure of (●) NO, (○) NO_2, and (◇) NO_x vs temperature over *ex*-[Fe,Al]MFI(a). Feed composition: 0.2 mbar of NO_2 in He; $P = 1$ bar; GHSV = 60,000 h^{-1}. Equilibrium composition of NO and NO_2 (Eq. [4]) is represented by dashed lines.

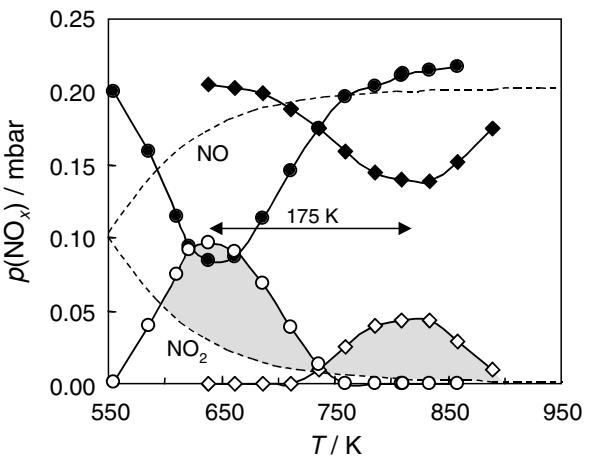

FIG. 9. Partial pressure of (●, ◆) NO and (○, ◇) NO_2 vs temperature over Fe-beta (circles) and Fe/Al_2O_3 (diamonds). Feed composition: 1.5 mbar of N_2O + 0.2 mbar of NO in He; $P = 1$ bar; GHSV = 60,000 h^{-1}. Equilibrium composition of NO and NO_2 (Eq. [4]) is represented by dashed lines.

temperature between the promoted and nonpromoted systems or by an increased N_2O conversion at the same temperature. The temperature shift in Fe–zeolites and Fe-supported oxides for 50% N_2O conversion is ~100 and ~50 K, respectively. In, e.g., Fe/ZSM-5 or Fe-beta, conversion increases from 10 to 100% at 698 K in the presence of NO, while the conversion over Fe/Al_2O_3 only increases from 10 to 30% at 823 K. The ion-exchanged catalysts are active in a temperature range similar to the *ex*-framework catalysts (compare Figs. 1 and 8a). Promotion of N_2O decomposition and formation of NO_2 over Fe/Al_2O_3 and Fe/SiO_2 take place at much higher temperatures. The last observation is derived from the NO_x profiles over these catalysts, which are shown in Fig. 9 for Fe-beta and Fe/Al_2O_3. Again the value of the partial NO and NO_2 pressure indicates that these are not controlled by the equilibrium in Eq. [4].

Multitrack Experiments

N_2O decomposition. Multitrack was used to further investigate the formation of O_2 during N_2O decomposition and the influence of NO in the N_2O conversion (O_2 formation) over *ex*-[Fe,Al]MFI(a). A typical Multitrack profile during direct N_2O decomposition at 823 K over this catalyst after 100 pulses is presented in Fig. 10. The N_2O and N_2 signals are very similar in shape. The O_2 response signal of the N_2O pulse, being much broader, deviates from the N_2O and N_2 signal. In order to determine whether the shape of

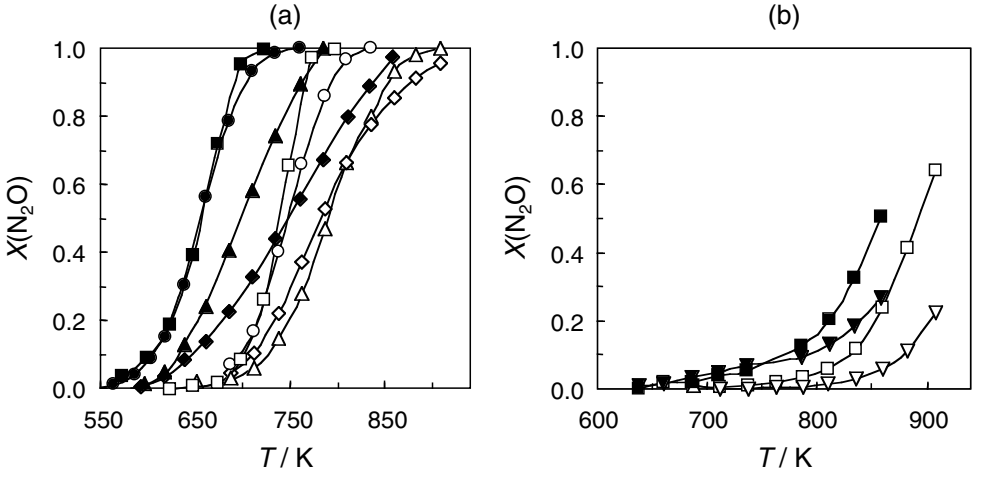

FIG. 8. N_2O conversion vs temperature over (a) low-temperature catalysts [(□, ■) Fe/ZSM-5, (△, ▲) Fe–ZSM-5, (○, ●) Fe-beta, (◇, ◆) Fe–USY] and (b) high-temperature catalysts [(□, ■) Fe/Al_2O_3 and (▽, ▼) Fe/SiO_2]. Feed composition: open symbols, 1.5 mbar of N_2O in He; solid symbols, 1.5 mbar of N_2O + 0.2 mbar of NO in He; $P = 1$ bar; GHSV = 60,000 h^{-1}.

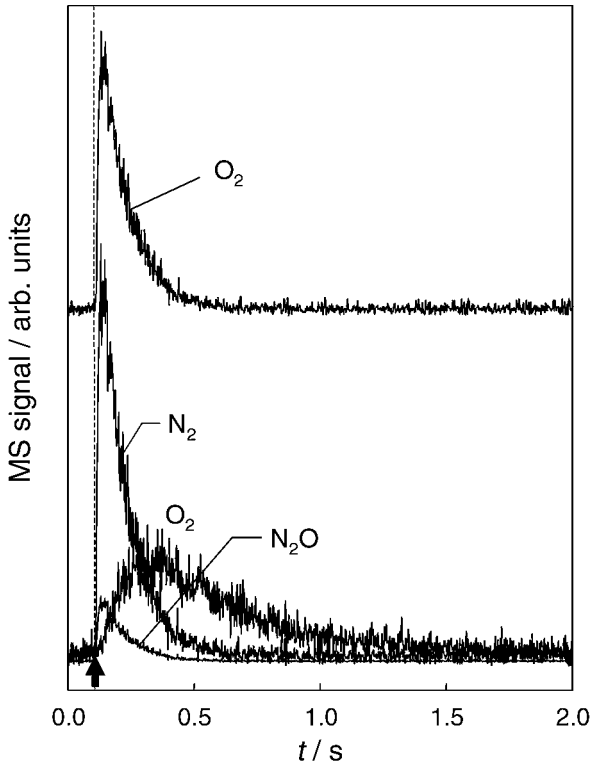

FIG. 10. Typical Multitrack profiles of N_2O, N_2, and O_2 during pulsing of pure N_2O (at 0.1 s) over *ex*-[Fe,Al]MFI(a) at 823 K. The upper profile results from separate experiments pulsing pure O_2 over the catalyst bed at the same temperature. Profiles recorded after 100 pulses.

the oxygen is due to a mechanistic feature of N_2O decomposition or simply due to nonreactive adsorption–desorption phenomena of O_2 along the catalyst bed, molecular oxygen was pulsed. In this case the pulse response is very similar in shape to that of N_2 and N_2O (Fig. 10), confirming the validity of the first hypothesis.

The delay of the oxygen signal was further investigated by pulsing N_2O at different reaction temperatures. These results are shown in Fig. 11. In the range 573–673 K, a very broad oxygen signal is observed. At 723 K the oxygen signal becomes more pronounced. Around 873 K the signal significantly sharpens, indicating that the rate of desorption of oxygen from the catalyst surface is significantly enhanced. Valuable information on the dynamic oxygen desorption process from the catalyst surface is also obtained from the desorption profiles of O_2 shown in Fig. 12. In these experiments, the O_2 decay signal is continuously monitored after stopping N_2O pulsing after 100 pulses at temperatures between 673 and 798 K. At 673 K, surface oxygen slowly desorbs from the catalyst surface at a constant rate over more than 25 s after stopping N_2O pulsing. Desorption is considerably faster at higher temperatures. At, e.g., 698 K, desorption takes ~15 s, decreasing to ~7 s at 723 K and so on. At 798 K, oxygen desorption is relatively fast (~5 s after stopping N_2O pulsing). This trend indicates the relative stability of the surface oxygen species with temperature.

NO-assisted N_2O decomposition. To study the effect of NO on the O_2 formation in N_2O decomposition, dual-pulse experiments were carried out at different temperatures, in which N_2O and NO were pulsed at 0.1 and 1 s, respectively, repeated in cycles of 2 s. The O_2 response in different stages of the experiment at 773 K is shown in Fig. 13. Pulsing N_2O (at 0.1 s) over *ex*-[Fe,Al]MFI(a) at this temperature leads to a broad oxygen signal (Fig. 13, profile a), indicating a relatively slow desorption of O_2. Alternate pulsing of N_2O and NO for 10 cycles leads to a remarkable effect on the O_2 response at the time of the N_2O pulse. The O_2 response sharpens (Fig. 13, profile b), indicating a significantly faster O_2 desorption in N_2O–NO cycles than in the experiment with only N_2O. Stopping NO pulsing results in a transition back to the original catalyst behavior in six cycles (12 s), with a very broad O_2 response (Fig. 13, profiles c and d). At lower temperatures the promotion effect lasts longer. At 698 K, the promotion is vanished 20 cycles (40 s) after stopping NO pulsing. This indicates that adsorbed species formed at the time of the NO pulse are involved in the enhanced O_2 formation and their stability toward desorption determines the duration of the effect. The sharp oxygen signal is rapidly recovered after four pulses of NO (Fig. 13, profiles e and f).

During the dual-pulse experiments at these temperatures, no NO or NO_2 signals were observed at the time of the N_2O pulse, which indicates that NO does not block N_2O decomposition sites. NO_2 formation was observed, but only at the time of the NO pulse (Fig. 13, profile g). The MS technique did not allow quantification of the NO_2 desorption. At high temperatures (e.g., 973 K) the effect of NO on the oxygen desorption behavior over *ex*-[Fe,Al]MFI(a) is negligible (21), since the O_2 profiles obtained by pulsing N_2O only, or N_2O and NO sequentially, are very similar. It should be noted that at such high temperature N_2O conversion over *ex*-[Fe,Al]MFI(a) was 100% both in the absence and in the presence of NO under flow conditions.

DISCUSSION

Role of the Structure of the Fe Species in NO-Assisted N_2O Decomposition

The nature of the active sites in Fe–zeolites (especially in FeMFI) prepared by various methods has already been discussed extensively in the literature (24–29). Isolated iron ions or oligonuclear oxo-iron species in the zeolite channels, as well as iron oxide particles (of different sizes and distributions), are generally identified in these heterogeneous systems. The nature and relative amounts of the various species depend on the preparation method, which determines the catalytic activity.

The different activities of the catalysts in Figs. 1, 2, and 8 should be related to the nature of the active site for N_2O activation. The strength of the Fe–O bond formed in the first step of the catalytic cycle (Eq. [1]) strongly depends on the nature of the iron species in the material, and here

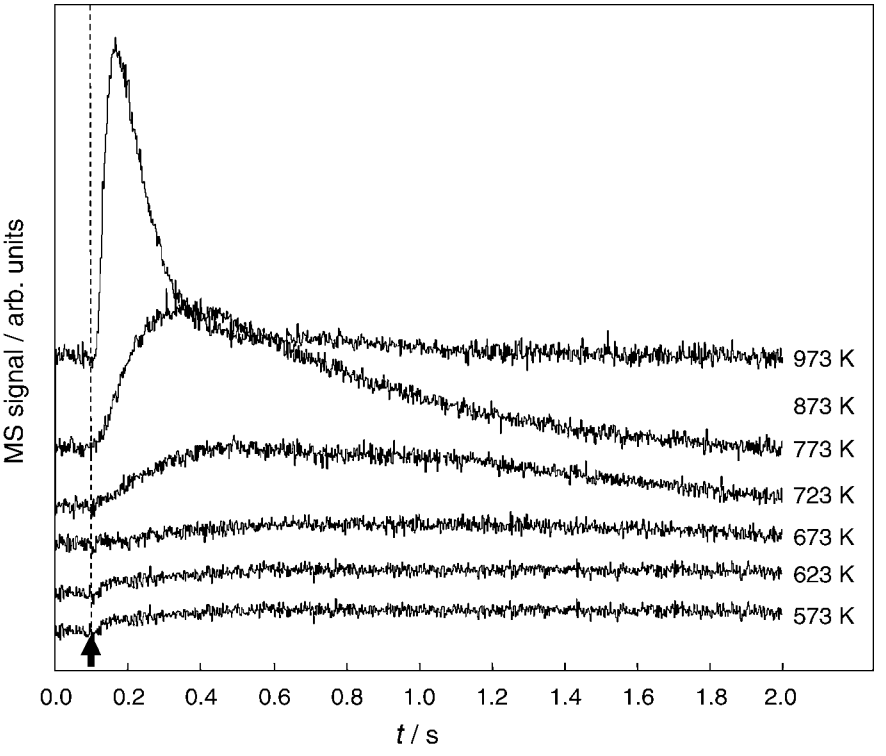

FIG. 11. O_2 profiles from Multitrack during continuous pulsing of pure N_2O (at 0.1 s) over *ex*-[Fe,Al]MFI(a) at different temperatures. Profiles recorded after 100 pulses.

the zeolite structure plays a crucial role in determining the specificity of these species. It is beyond the scope of the present paper to discuss the exact nature of the active site in N_2O decomposition, although it is a highly challenging issue for catalysis.

In view of the heterogeneous nature of the catalyst formulations with respect to iron, it is not surprising that the promoting effect of NO on N_2O decomposition has been identified for zeolite catalysts of different constitutions (e.g., those prepared via an *ex*-framework route vs the

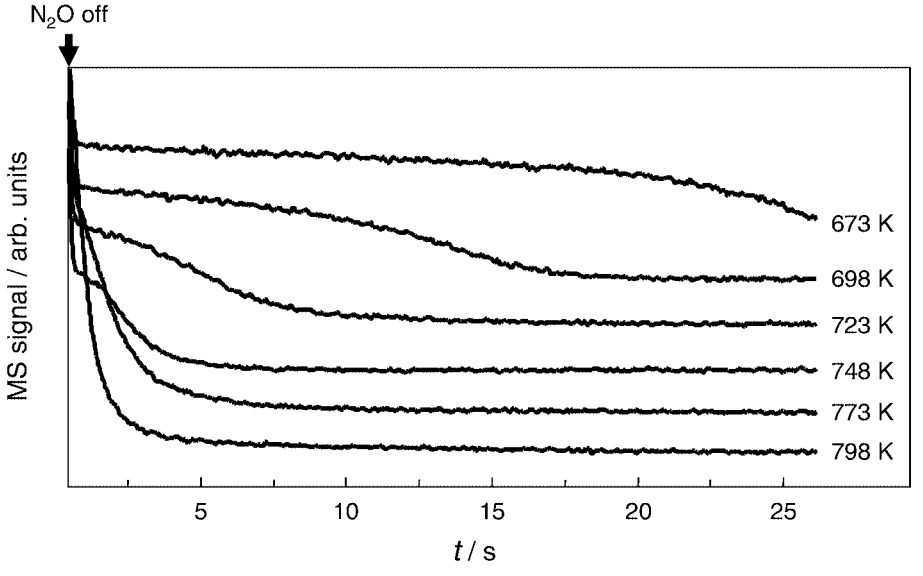

FIG. 12. Oxygen desorption profiles measured by Multitrack after stopping N_2O pulses (N_2O off) over *ex*-[Fe,Al]MFI(a) at different temperatures. Pulses were stopped after 100 pulses of the gas, using a cycle time of 2 s.

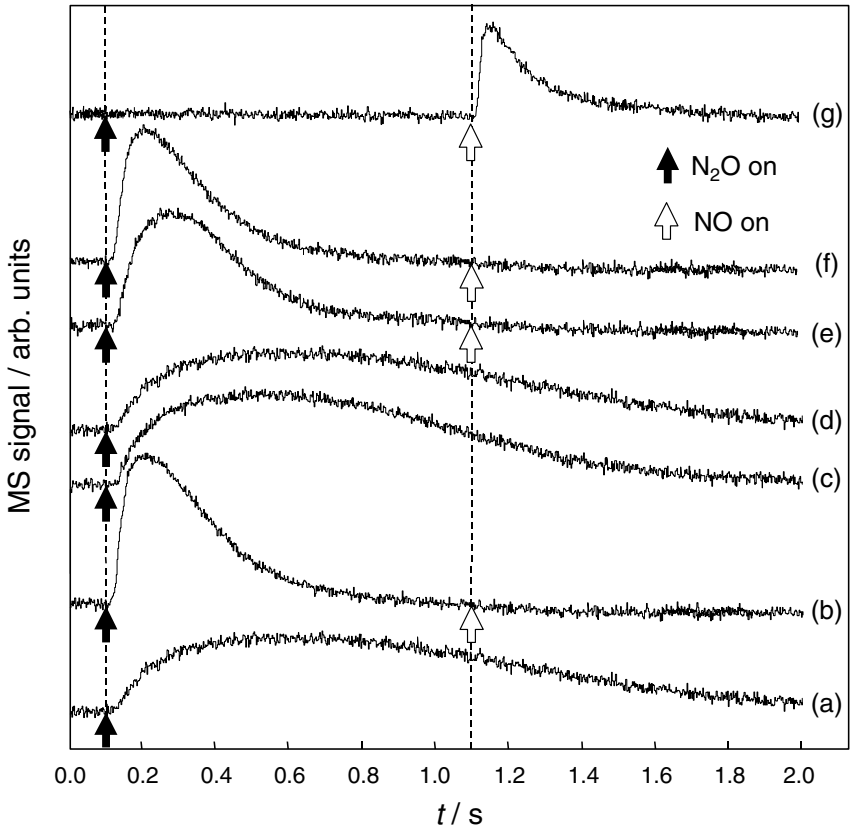

FIG. 13. O_2 profiles measured by Multitrack during catalytic decomposition of N_2O over *ex*-[Fe,Al]MFI(a) at 773 K using a cycle time of 2 s: (a) pulsing N_2O (at 0.1 s) after 100 cycles; (b) subsequent pulsing N_2O (at 0.1 s) and NO (at 1.1 s) after 10 cycles; (c, d) pulsing N_2O only (at 0.1 s), three and five cycles after switching off the NO valve, respectively; (e, f) pulsing N_2O (at 0.1 s) and NO (at 1.1 s), two and four cycles after switching on the NO valve, respectively. (g) A typical NO_2 profile during pulsing N_2O (0.1 s) and NO (1.1 s) after 100 cycles.

catalysts prepared by ion-exchange or sublimation methods). Even Fe catalysts on conventional supports (Al_2O_3, SiO_2), prepared by incipient wetness impregnation, also show an improved activity. In the latter catalysts iron is basically present as iron oxide particles (in a wide distribution of sizes). Apparently, the NO promotion is not specific for a certain type of Fe species. This is most likely the result of the high affinity of NO to reduced Fe sites, irrespective of the local structure of these sites. The high affinity of NO for reduced Fe sites has been demonstrated in various infrared studies, the absorption frequencies being assigned to different Fe configurations present in zeolites and located on conventional supports (21, 30–32). The order in activity of the different catalysts is not changed after addition of NO, which indicates a certain uniformity of the active sites promoted by NO. So, alternatively the activity and promotion effect may be attributed to the same active species, present in different amounts in the various catalysts.

Mechanism of NO-Assisted N_2O Decomposition

N_2O decomposition. As indicated in the Introduction, the beneficial effect of NO on the activity of FeZSM-5 has been attributed by Kapteijn *et al.* (20, 33) to scavenging of adsorbed oxygen (O^*), regenerating the active site (Eq. [2]). In a recent paper we demonstrated that scavenging of adsorbed O^* by NO is not the only mechanism of promotion, and that NO also enhances O_2 formation (21), acting as a catalyst. Multitrack experiments presented here show that oxygen desorbs from the catalyst surface in a relatively slow step. Scheme 1 shows a typical reaction pathway for catalytic N_2O decomposition (12), including the transition between the structures involved (Scheme 1, structures I–III). First, a vacant site (□) is oxidized by reaction with N_2O (reaction [1.1]), leading to O□ species (unambiguously denoted as O^*). The reaction of a second N_2O molecule with the oxidized site results in the regeneration of the sites, according to reaction [1.2]. Oxygen desorption can also take place by recombination of adsorbed oxygen atoms (reaction [1.3]). In view of the slow oxygen desorption (Figs. 11 and 12), the recombination of two oxygen atoms (located on two different sites) appears the most likely explanation for O_2 formation. These oxygen atoms can be originally separated, i.e., deposited at remote iron sites (Scheme 1, structure III). The dynamic nature of the adsorbed oxygen in the zeolite was studied by Hall and

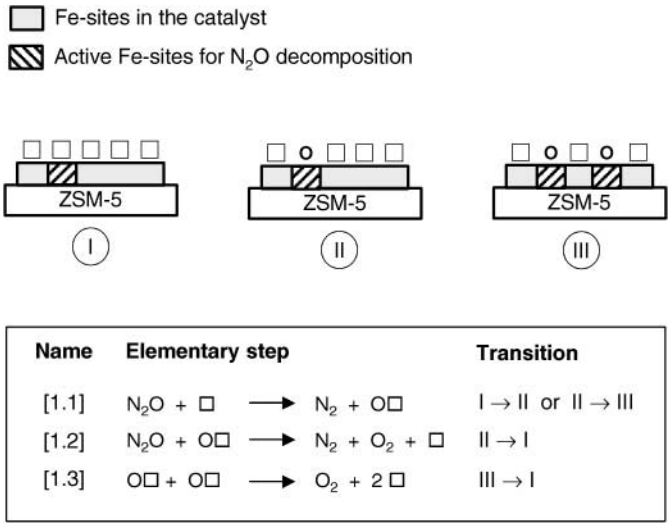

Name	Elementary step	Transition
[1.1]	$N_2O + \square \rightarrow N_2 + O\square$	$I \rightarrow II$ or $II \rightarrow III$
[1.2]	$N_2O + O\square \rightarrow N_2 + O_2 + \square$	$II \rightarrow I$
[1.3]	$O\square + O\square \rightarrow O_2 + 2\square$	$III \rightarrow I$

SCHEME 1. Schematic representation of a typical N_2O decomposition mechanism.

coworkers (34) by step-switching experiments from N_2O to $N_2{}^{18}O$ over Fe–Mor. These studies showed that adsorbed ^{18}O species (deposited by $N_2{}^{18}O$) in Fe–Mor can exchange with the lattice oxygen of the zeolite in the vicinity of the Fe; so the oxygen must have a certain mobility to achieve this. The slow oxygen desorption in Fe–zeolites can then be understood by a slow migration of adsorbed oxygen atoms. The rate of desorption is higher at higher temperatures (Figs. 11 and 12) and is attributed to a higher oxygen mobility and recombination. Once adsorbed atomic O^* species meet each other, desorption takes place rapidly, since no O_2 adsorption was observed for Fe–ZSM-5 (12, 35, 36).

NO-assisted N_2O decomposition. The rate of oxygen desorption from the catalyst surface is greatly enhanced by NO addition. Indeed, a significant increase was found in the amount of oxygen formed if NO was added to the N_2O-containing feed (Fig. 13), and only a relatively small amount of NO is needed to dramatically increase the N_2O decomposition rate (Fig. 3). Although during this process NO_2 is formed, even beyond the thermodynamic equilibrium between NO, O_2, and NO_2 according to Eq. [4] (see, e.g., Fig. 4), the enhanced oxygen production strongly suggests a catalytic effect of NO. If Eq. [2] was the only promotion route induced by the addition of NO, a progressive increase in conversion upon increasing the inlet NO partial pressure would be expected. This is not the case; the promotion occurs already at relatively low substoichiometric amounts of NO, indicating the catalytic nature, and reaches a limiting value at increasing molar NO/N_2O feed ratios up to 10. This suggests the involvement of NO adsorption, and that the sites where NO is adsorbed are not in competition with N_2O decomposition sites. Competitive adsorption would have resulted in inhibition, especially at high partial NO pressures. From the observation that at 698 K only four NO pulses are needed to restore the promotion effect, the pulse size, and the amount of catalyst used, and assuming that all NO remains adsorbed at Fe sites, it can be calculated that less than 0.9% of the Fe present is involved in the promotion. This also suggests that a very low fraction of the Fe is active in the reaction.

Promotion by NO induces a significant decrease, ~45–55 kJ · mol^{-1}, in the apparent activation energy for N_2O decomposition, which has also been observed in the reaction of N_2O and CO (with respect to direct N_2O decomposition) over ion-exchanged transition metal (Fe, Co, Cu) ZSM-5 catalysts (33), suggesting a similar effect on the reaction mechanism, i.e., the removal of oxygen from the active site.

What the relative contribution is of enhanced oxygen desorption vs the formation of NO_2 over the catalysts needs some further discussion. At relatively low temperatures the first phenomenon is stronger than at high temperatures, as indicated by the Multitrack analyses. Above 900 K the oxygen response in the case of the *ex*-[Fe,Al]MFI(a) at the N_2O pulse is no longer affected by alternating N_2O–NO pulsing (21). To explain the enhancement of the O_2 desorption rate at the time of the N_2O pulse, an adsorbed species formed at the time of the NO pulse needs to be involved. The amount of adsorbed NO will be reduced at high temperatures, while oxygen desorption at high temperatures already proceeds fast. This adsorption involvement is supported by the slower decay of the NO promotion at lower temperatures in the dual-pulse Multitrack experiments after stopping NO pulsing.

The absence of the enhanced O_2 desorption effect at high temperatures is in agreement with the relatively smaller promoting effect of NO on the performance of metal oxide (Al_2O_3, SiO_2)-supported Fe catalysts vs zeolitic Fe catalysts. In the former catalytic systems, it is likely that removal of O^* by NO, as stated in Eq. [2], plays a more important role in the promotion than enhanced O_2 desorption. Sang and Lund (14) use the interconversion of nitrates and nitrites to explain the enhancement of N_2O conversion by NO. However, for Al_2O_3- and SiO_2-supported Fe catalysts this explanation does not appear very likely, since nitrites and nitrates are not stable at the conditions where the promoting effect is observed. Furthermore, in an infrared analysis of the Fe catalysts (21), nitrate bands have never been observed, only adsorbed NO and NO_2 species.

Although NO_2 is decomposed over Fe-based catalysts into NO and O_2, the contribution of NO_2 decomposition to the formation of O_2 in the NO-assisted N_2O decomposition is likely to be limited. The Multitrack experiments clearly show that oxygen desorption is triggered at the time of the N_2O pulse, and not at the time of the NO pulse. NO_2 formation is observed at the time of the NO pulse, indicating displacement of adsorbed NO_2 by NO, as confirmed by recent transient *in situ* FT-IR/MS studies over *ex*-[Fe,Al]MFI(a) (21). In the Multitrack, formation of O_2 and NO_2 is decoupled: NO_2 is mainly released due to

displacement by NO and probably by thermal desorption, while O_2 is formed during the N_2O pulses. If NO_2 decomposition, like that presented in Fig. 7, contributed significantly to O_2 formation, an O_2 response would have been expected at the time of the NO pulse, rather than at the time of the N_2O pulse only. This excludes Eq. [3] as a major cause of the promotion effect.

Reaction pathways and proposed mechanism. In view of the results presented in this paper and elsewhere (21), various pathway(s) are needed to explain the catalytic effect of NO on the N_2O decomposition. The different experimental observations are depicted in Scheme 2. The transitions of the different structures considered (Scheme 2, structures I–IV) are also considered in the reaction mechanism. Initially, N_2O reacts on a vacant site, yielding N_2 and leaving an oxidized site (reaction [2.1]). On the catalyst, a substantial amount of adsorbed NO is present, as previously observed by *in situ* FT-IR (21). Due to the absence of inhibition by NO in the activity tests and the fact that no NO signal appears at the time of the N_2O pulse in the Multitrack experiments, it is concluded that the NO adsorption and N_2O decomposition do not compete for the same site, so both processes occur at different Fe species (solid grey area and crosshatched area in Scheme 2). Adsorption of N_2O (as O*) and NO in two open coordinations at the same iron site seems hardly probable, since dinitrosyls were not identified by infrared studies in this system. The production of NO_2 is shown in reaction [2.2] (Scheme 2), which is likely the major mode of promotion for high-temperature catalysts, i.e., Fe/Al_2O_3 and Fe/SiO_2. For low-temperature Fe–zeolite catalysts, N_2O activation occurs next to an adsorbed NO molecule (*NO). At these lower temperatures (550–700 K) the oxidized site (O□) subsequently oxidizes adsorbed NO to adsorbed NO_2 (reaction [2.3]), yielding structure III in Scheme 2. Subsequently, NO_2 desorption is induced by adsorption of NO (reaction [2.4]), as was observed from the Multitrack experiments by the presence of a NO_2 signal at the time of the NO pulse. This closes the catalytic cycle for the conversion of N_2O and NO to N_2 and NO_2 at lower temperatures.

Different options can be proposed to explain the enhanced oxygen formation. Again N_2O activation occurs next to an adsorbed NO molecule, yielding structure II in Scheme 2. Subsequently a second N_2O molecule reacts with the site, yielding N_2 and O_2 (reaction [2.5]), and structure I is regenerated. The enhanced oxygen desorption from the active center has been ascribed to a reduced stability of adsorbed oxygen, induced by either electronic or steric effects of the NO adsorbed on neighboring oxidized sites (21). A more plausible explanation for the enhanced oxygen desorption is reaction [2.6]. The increased N_2O decomposition is simply explained by the recombination of oxygen present in adsorbed NO_2 and oxygen species deposited by N_2O on a neighboring site.

Thus the adsorbed NO serves to accommodate temporarily the deposited oxygen from the N_2O, freeing the neighboring site for deposition of a second oxygen. This would imply the presence of remote sites for the N_2O decomposition. Consequently, the migration of oxygen atoms to recombine to molecular oxygen constitutes the

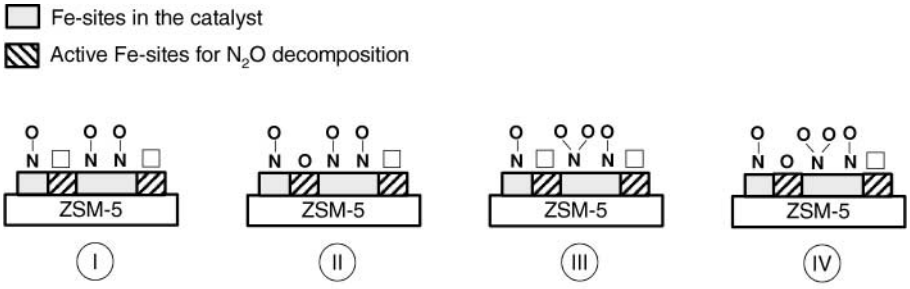

Name	Elementary step			Transition
[2.1]	$N_2O + \square$	⟶	$N_2 + O\square$	I → II
[2.2]	$NO + O\square$	⟶	$NO_2 + \square$	II → I
[2.3]	$*NO + O\square$	⟶	$*NO_2 + \square$	II → III
[2.4]	$NO + *NO_2$	⟶	$NO_2 + *NO$	III → I
[2.5]	$N_2O + O\square$	⟶	$N_2 + O_2 + \square$	II → I
[2.6]	$*NO_2 + O\square$	⟶	$*NO + O_2 + \square$	IV → I
[2.7]	$*NO_2 + \square$	⟶	$*NO + O\square$	III → II

SCHEME 2. Possible pathways in the NO-assisted N_2O decomposition over *ex*-[Fe,Al]MFI(a).

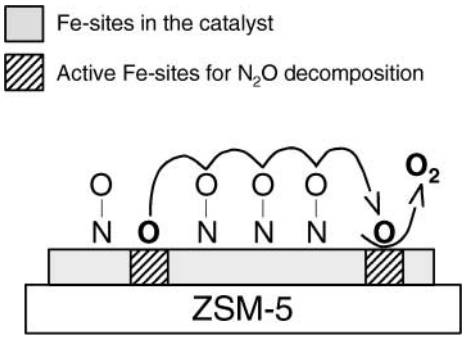

SCHEME 3. Proposed NO-assisted oxygen desorption mechanism during N_2O decomposition.

rate-determining process in N_2O decomposition. Taking this further, it could be speculated that the presence of NO on the catalyst surface enhances the mobility of adsorbed oxygen via intermediate NO_2 species. This mechanism, schematically depicted in Scheme 3, leads to a faster oxygen recombination, and thus an accelerated O_2 desorption. The transfer of the oxygen atom from one NO to the other is well possible, as previously observed for NO and $^{15}N^{18}O$ step changes over Cu–ZSM-5 and Cu–Y (34, 37). Of course, the O_2 formation by two adjacent adsorbed NO_2 groups cannot be ruled out.

Finally the observed NO_2 decomposition over *ex*-[Fe,Al]MFI(a) and in general Fe–zeolites (reaction [2.7] in Scheme 2) in flow experiments deserves some discussion. It has been proposed that N_2O decomposition over Fe–zeolites yields the so-called α-oxygen (9), which has the ability to selectively oxidize benzene in phenol. Since the Fe–zeolites are able to convert NO_2 into NO and O_2 at relative high rates, i.e., equilibrium is attained at 700 K, it could be hypothesized on the basis of the proposed schemes that NO_2 is also able to produce adsorbed (atomic) oxygen species (from structure III to II in Scheme 2). So in principle it could be used as selective oxidant. A drawback, however, will be that the catalyst also effectively helps the O_2 formation, thus rendering NO_2 into a less efficient reactant than N_2O. Alternatively, mixtures of O_2 and NO could be used.

The results in this paper have implications for the application of N_2O in selective oxidations. In the AlphOx^{TM} process (38), the N_2O originates as a coproduct of the oxidation of cyclohexanone/cyclohexanol mixtures by nitric acid. This N_2O contains also NO. It is clear that this NO has to be removed to large extent otherwise it will lower considerably the utilization of N_2O in the benzene oxidation by providing an escape route for the so-called α-oxygen from the N_2O. This can be translated into an accelerated oxygen desorption and/or the sequestration of reactive O* as adsorbed $^*NO_x$ species, impeding the effective transfer of atomic oxygen to the benzene molecule.

The isolated nature of the sites prohibits the dissociation of O_2 explaining the absence of O_2 inhibition. The formation of NO_2 beyond thermodynamic equilibrium of Eq. [4] indicates that Eq. [3] proceeds faster than Eq. [4] under competitive conditions, where NO, N_2O, O_2, and NO_2 are simultaneously present. The NO_2 formation is in fact due to the displacement by NO, which adsorbs stronger (21). Hence, O_2 formation by adjacently adsorbed NO_2 will be suppressed under these circumstances, but could explain the results of Fig. 7 in the absence of N_2O. Alternatively, O_2 formation from NO_2, via reaction [2.6], requires the competition between N_2O and NO_2 to oxidize a vacant (□) site. If N_2O is a more efficient oxidizer of these sites, NO_2 levels beyond thermodynamic equilibrium of Eq. [4] are well feasible.

At this point it is worth noting two other catalyzed reactions where NO serves as an "atomic" oxygen transport facilitator. The first is the old lead chamber process for SO_2 oxidation, in which NO acts as a gaseous carrier (39). The second is the role of NO in the bifunctional catalysis to oxidize soot (40, 41). There a catalyst, e.g., metal oxide (Cr_2O_3, Co_3O_4, CuO) or Pt based, oxidizes NO with O_2 to NO_2 and the latter oxidizes the soot at temperatures where O_2 is not active. Although in these examples the oxygen is transported through the gas phase, in the current study this occurs via an adsorbed mode. As mentioned before this property of NO may be utilized in other (selective) oxidation reactions.

CONCLUSIONS

NO strongly promotes N_2O decomposition over Fe-based catalysts. The promoting effect is observed for many different formulations and appears independent on the nature of the bulk of the Fe species in the catalyst. The temperature at which N_2O decomposition occurs is strongly dependent on the catalyst. Small amounts of NO in the feed ($NO/N_2O < 0.25$) are sufficient to produce a substantial increase in N_2O conversion for all the catalysts. Higher partial NO pressures ($NO/N_2O > 0.25$) lead to a saturation behavior of the N_2O conversion, although no inhibition by NO is observed, even at $NO/N_2O = 10$. Apparently, different sites are involved in the NO adsorption and the deposition of oxygen by N_2O. The latter sites seem to be remote from each other, rendering the oxygen atom recombination the rate-determining process. High temperatures stimulate this process but also adsorbed NO at lower temperatures. Adsorbed NO may temporarily accommodate oxygen deposited by N_2O on a neighboring site, allowing the deposition of a second oxygen and the recombination of both. Less than 0.9% of the Fe seems to participate in this promotion, indicating the low density of active sites. Additionally, adsorbed NO may facilitate the migration of

oxygen through NO_2 intermediates, enhancing the change of recombination to O_2.

ACKNOWLEDGMENTS

This research was financially supported by the Dutch Council for Chemistry Research (CW-NWO). B. vd. Linden and S. Mollá-Romano are acknowledged for their assistance in the Multitrack measurements. Prof. Dr. Ir. A. Bliek is acknowledged for the use of the *in situ* FT-IR cell.

REFERENCES

1. Feng, X., and Hall, W. K., *Catal. Lett*. **41**, 45 (1996).
2. Chen, H.-Y., and Sachtler, W. M. H., *Catal. Today* **42**, 73 (1998).
3. Ma, A.-Z., and Grünert, W., *Chem. Commun.* 71 (1999).
4. Long, R. Q., and Yang, R. T., *J. Catal*. **188**, 332 (1999).
5. Kögel, M., Mönnig, R., Schwieger, W., Tissler, A., and Turek, T., *J. Catal*. **182**, 470 (1999).
6. Pophal, C., Yogo, T., Yamada, K., and Segawa, K., *Appl. Catal. B* **16**, 177 (1998).
7. Centi, G., and Vazanna, F., *Catal. Today* **53**, 683 (1999).
8. Mauvezin, M., Delahay, G., Kißlich, F., Coq, B., and Kieger, S., *Catal. Lett*. **62**, 41 (1999).
9. Panov, G. I., Uriarte, A. K., Rodkin, M. A., and Sobolev, V. I., *Catal. Today* **41**, 365 (1998).
10. Dubkov, K. A., Sobolev, V. I., and Panov, G. I., *Kinet. Catal*. **39**, 72 (1998).
11. Ribera, A., Arends, I. W. C. E., de Vries, S., Pérez-Ramírez, J., and Sheldon, R. A., *J. Catal*. **195**, 287 (2000).
12. Kapteijn, F., Rodríguez-Mirasol, J., and Moulijn, J. A., *Appl. Catal. B* **9**, 25 (1996).
13. El-Malki, E-M., van Santen, R. A., and Sachtler, W. M. H., *J. Catal*. **196**, 212 (2000).
14. Sang, C., and Lund, C. R. F., *Catal. Lett*. **73**, 73 (2001).
15. Long, R. Q., and Yang, R. T., *Chem. Commun*. 1651 (2000).
16. Pérez-Ramírez, J., Kapteijn, F., Mul, G., and Moulijn, J. A., *Chem. Commun*. 693 (2001).
17. Pérez-Ramírez, J., Kapteijn, F., Mul, G., and Moulijn, J. A., *Appl. Catal. B* **35**, 227 (2002).
18. Oi, J., Obuchi, A., Bamwenda, G. R., Ogata, A., Yagita, H., Kushiyama, S., and Mizuno, K., *Appl. Catal. B* **12**, 277 (1997).
19. Centi, G., Galli, A., Montanari, B., Perathoner, S., and Vaccari, A., *Catal. Today* **35**, 113 (1997).
20. Kapteijn, F., Mul, G., Marbán, G., Rodríguez-Mirasol, J., and Moulijn, J. A., *Stud. Surf. Sci. Catal*. **101**, 641 (1996).
21. Mul, G., Pérez-Ramírez, J., Kapteijn, F., and Moulijn, J. A., *Catal. Lett*. **77**, 7 (2001).
22. Pérez-Ramírez, J., Berger, R. J., Mul, G., Kapteijn, F., and Moulijn, J. A., *Catal. Today* **60**, 93 (2000).
23. Nijhuis, T. A., van den Broeke, L. J. P., Linders, M. J. G., Makkee, M., Kapteijn, F., and Moulijn, J. A., *Catal. Today* **53**, 189 (1999).
24. Lobree, L. J., Hwang, I.-C., Reimer, J. A., and Bell, A. T., *J. Catal*. **186**, 242 (1999).
25. Marturano, P., Drozdová, L., Kogelbauer, A., and Prins, R., *J. Catal*. **192**, 236 (2000).
26. Battiston, A. A., Bitter, J. H., and Koningsberger, D. C., *Catal. Lett*. **66**, 75 (2000).
27. Joyner, R., and Stockenhuber, M., *J. Phys. Chem. B* **103**, 5963 (1999).
28. Long, R. Q., and Yang, R. T., *J. Catal*. **194**, 80 (2000).
29. Pérez-Ramírez, J., Mul, G., Kapteijn, F., Moulijn, J. A., Overweg, A. R., Doménech, A., Ribera, A., and Arends, I. W. C. E., *J. Catal*. **207**, 113 (2002).
30. Lobree, L. J., Hwang, I.-C., Reimer, J. A., and Bell, A. T., *Catal. Lett*. **63**, 233 (1999).
31. Hadjiivanov, K., Knözinger, H., Tsyntsarski, B., and Dimitrov, L., *Catal. Lett*. **62**, 35 (1999).
32. Lezcano, M., Kovalchuk, V. I., and d'Itri, J. L., *Kinet. Catal*. **42**, 104 (2001).
33. Kapteijn, F., Marbán, G., Rodríguez-Mirasol, J., and Moulijn, J. A., *J. Catal*. **167**, 256 (1997).
34. Valyon, J., Millman, W. S., and Hall, W. K., *Catal. Lett.* **24**, 215 (1994).
35. Sobolev, V. I., Panov, G. I., Kharitonov, A. S., Romannikov, V. N., Volodin, A. M., and Ione, K. G., *J. Catal.* **139**, 435 (1993).
36. Boreskov, G. K., *in* "Catalysis: Science and Technology" (J. R. Anderson and M. Boudart, Eds.), Vol. 3, p. 39. Springer-Verlag, Berlin, 1982.
37. Valyon, J., and Hall, W. K., *J. Catal*. **143**, 520 (1993).
38. Notté, P. P., *Topics Catal*. **13**, 387 (2000).
39. Muller, T. L., "Kirk–Othmer Encyclopedia of Chemical Technology." (M. Howe-Grant, Ed.), 4th ed., Vol. 23, p. 363. Wiley, New York, 1997.
40. Mul, G., Zhu, W., Kapteijn, F., and Moulijn, J. A., *Appl. Catal. B* **17**, 205 (1998).
41. Jelles, S. J., Makkee, M., and Moulijn, J. A., *Topics Catal*. **16/17**, 269 (2001).